Research Square

Preprints are preliminary reports that have not undergone peer review.
They should not be considered conclusive, used to inform clinical practice,
or referenced by the media as validated information.

Plant-based green fabrication of S-scheme CuO/CdO/bentonite heterojunction with enhanced photocatalytic performance for degradation of levofloxacin

Majid Mahjoore
University of Birjand
Moones Honarmand (honarmand.moones@yahoo.com)
Birjand University of Technology
Ahmad Aryafar
University of Birjand

Research Article

Keywords: Bentonite, S-scheme heterojunction, Photocatalysis, Levofloxacin, Sunlight

Posted Date: August 2nd, 2022

DOI: https://doi.org/10.21203/rs.3.rs-1887737/v1

License: This work is licensed under a Creative Commons Attribution 4.0 International License.
Read Full License

Abstract

In this research, for the first time, CuO and CdO nanoparticles (NPs) were synthesized and anchored on layered bentonite using *Ferula* persica in the interest of developing a novel S-scheme nano-heterojunction (denoted as CuO-CdO-BT). *Ferula* persica acted as a naturally-sourced reducing agent and stabilizer for the synthesis of NPs. The performance of CuO-CdO-BT was evaluated for the degradation of levofloxacin from aqueous solution under sunlight. The bentonite as a support not only reduced the agglomeration of CuO and CdO NPs, but also decreased the size of biosynthesized NPs, which in turn increased the active surface of NPs and the photodegardation efficiency. The effect of operational reaction system variables was examined in an attempt to optimize the photocatalytic capability of CuO-CdO-BT. Under optimum conditions (catalyst dosage = 0.4 g/L, LVF concentration = 10 mg/L and pH = 8), 96.11% of levofloxacin was degraded using CuO-CdO-BT after 30 min with degradation kinetic of 0.108 min^{-1}, which was about 2.4 and 4.2 times higher than those of bare CuO and CdO NPs, respectively. The prominent role of superoxide radicals ($O_2^{\bullet -}$) and hydroxyl radicals ($^{\cdot}OH$) was determined in the photocatalytic reaction by the radical quenching experiments. The possible levofloxacin pathways were suggested based on the HPLC-MS analysis. High stability was demonstrated for biosynthesized photocatalyst during recycling experiments and 88.56% degradation efficiency was obtained after three cycles of photodegradation. The unique structural features of the new generation of S-scheme heterojunction and green synthesis of NPs using plant provide promising photocatalysts with synergistic features to improve wastewater treatment.

1. Introduction

Fluoroquinlone is a well-known synthetic antibiotic which has been utilized as an efficient antibacterial drug in the medication of many infectious ailments[1]. The US Food and Drug Administration reports that the total amount of consumed Fluoroquinolones is about 24,176 $(kg)^2$ in 2020. Levofloxacin is the second generation of fluoroquinolones, which is listed as one of the most widely used antibiotics due to its unique properties in the treatment of dysentery, tuberculosis and HIV[2]. However, recent studies have illustrated that levofloxacin is not fully metabolized in human and animal bodies and released into the wastewater through faces and urine[3]. Unfortunately, the traditional water treatment process cannot effectively degrade levofloxacin. The presence of this antibiotic in the environment raises widespread concerns about potential harm to public health and aquatic life. As a result, the development of effective treatment technologies for the complete degradation of antibiotics is an important necessity. Recently, the advanced oxidation processes in the presence of heterogeneous photocatalysts has emerged as an important and universally accepted technique for the efficient degradation of antibiotics[4, 5]. In this technique, semiconductor mediated photocatalysis is recognized as a promising tool due to its excellent performance and chemical-free approach.

The metal oxide nanoparticles (NPs) recently attracted tremendous attention as photocatalyst in eliminating organic pollutants from water bodies due to unique properties such as simplicity, high oxidation ability, mild reaction conditions, cost-effectiveness and excellent activity even at low amount of

the photocatalyst[6–9]. Among the various metal oxide nanoparticles, CuO NPs as p-type semiconductor are a good candidate for the removal of pharmaceutical contaminants because of their attractive properties including high chemical and physical stability, availability and simple preparation with different morphologies[10, 11]. In addition to all the mentioned advantages, the effective utilization of CuO NPs to remove antibiotics is limited in the range of short visible light absorption. The reason for this restriction is the broad bandgap of CuO NPs [12]. Also, high recombination rate of photo generated electron-hole pairs lead to a decrease in amount of reactive species for the oxidation of organic compounds and ultimately reduce the degradation efficiency. To enhance the use of natural sunlight and improve the separation efficiency of photo-induced electron-hole pairs, researchers have adopted a number of strategies such as the fabrication of heterostructure by coupling with other semiconductors and doping with metals and non-metals[13, 14]. One of the best ways is the construction of heterojunction between semiconductors with suitable band alignment through step scheme (S-scheme) electron-hole transfer model. In S-scheme heterojunction model, which was recently introduced for the first time in 2019, the recombination of electron-hole pairs are accelerated at the low potentials, but on the contrary, are inhibited at high potentials[15]. In other words, after light irradiation, the electrons in conductive band (CB) of one semiconductor with higher positions of CB and valence band (VB) recombine with the holes in VB of the other semiconductor with lower positions of CB and VB. In this way, useless electrons and holes are removed *via* recombination, while the strong oxidative photo-induced electrons in CB and holes in VB are preserved [16]. Therefore, the construction of S-scheme heterojunction is an efficient route to enhance the photocatalytic performance.

In order to design S-scheme heterojunction, CuO NPs can be combined with other semiconductors for construction of the novel nanocomposites[17]. Cadmium oxide (CdO) NPs thanks to some benefits like high chemical and physical stability, cost-effectiveness, non-toxicity and n-type narrow bandgap is among promising semiconductors to fabricate p-n heterojunction nanocomposites with CuO NPs[18].

Although NPs play an important role in the removal of pollutants, but agglomerate and their separation problems during work cannot be ignored. To ameliorate these drawbacks, the NPs are dispersed or full-grown onto solid supports such as silica[19], chitosan[20], starch [21] zeolite[22], carbon nanotube[23], and graphene oxide[24, 25]. Some of these supports are expensive and difficult to access. Bentonite (BT) is a plentiful and economical natural clay mineral[26]. Luckily, the high specific surface area and layered structure of BT can effectively prevent agglomeration and even recombination of photogenerated electron-hole pairs, thereby increasing the photocatalytic activity of nanoparticles[27, 28]. Thus, *in-situ* growth of CuO and CdO NPs onto bentonite lead to an economical eco-friendly nanocomposite for the effective photodegradation of pharmaceutical contaminants.

Due to the widespread use of nanoparticles in various fields, different methods for their synthesis have been proposed[29]. Most of these methods are costly and time consuming and, most importantly produce harmful waste. Hence, relying on environmental protection, recently, the various research communities have synthesized nanoparticles through green routes[30, 31]. The plants-assisted synthesis technique of

nanoparticles not only prohibit the use of toxic solvents and chemicals, but also control the release of hazardous by-products into wastewater.

Inspired from this green approach, herein, the environmentally-friendly and cost-effective copper oxide/cadmium oxide/bentonite (CuO-CdO-BT) S-scheme nano-heterojunction is synthesized using *Ferula* persica. *Ferula* persica, also known *as Ferula*, effectively acts as a green reducing and capping agent for the biosynthesis of CuO and CdO NPs. To the best of our knowledge, this is the first report for the green synthesis of S-scheme nano-heterojunction photocatalyst using plants extract. In the following, to eliminate drug contamination, the CuO-CdO-BT is utilized for the degradation of levofloxacin. As anticipated, the combination of CuO and CdO NPs with bentonite as an efficient S-scheme heterojunction shows superior photocatalytic performance and stability in the photodegaradion of LVF under natural sunlight. The obtained results display that the CuO-CdO-BT has a better photocatalytic performance compared with pure CuO NPs and CdO NPs. The key environmental operating parameters such as solution pH, concentration of LVF and catalysts dose are evaluated and fixed optimized condition. Furthermore, impact of the presence of various anions and scavengers are investigated on the photodegradation efficiency of LVF. Also recyclability test are studied. Finally, the pathways of LVF degradation and the charge transfer in CuO-CdO-BT are suggested.

2. Experimental Section

2.1. Materials and characterization

The used chemicals and apparatus in this study were provided in Supplementary materials.

2.2. Plant-based green fabrication of CuO-CdO-BT nano-heterojunction

The fabrication process of the CuO-CdO-BT nano-heterojunction using *Ferula* was described as below. Bentonite (0.2 g), $Cd(NO_3)_2.4H_2O$ aqueous solution (50 mL, 0.1 M, 1.542 g) and $CuSO_4.5H_2O$ aqueous solution (50 mL, 0.1 M, 1.245 g) were vigorously stirred for 30 minutes at room temperature. The *Ferula* aqueous extract (100 mL) was slowly added to the above well-mixed mixture for 30 minutes. The resulting mixture was kept stirring for 2 h at 80°C under reflux conditions. After cooling to laboratory temperature, the formed precipitates was rinsed multiple times with water to remove impurities and dried. In the end, the obtained powder was calcined in an electric furnace at 500°C for 2 hours. For comparative purposes, pure CuO and CdO NPs were produced under similar conditions without the use of bentonite as well as $Cd(NO_3)_2.4H_2O$ and $CuSO_4.5H_2O$, respectively.

2.3. Photocatalytic experiments

The photocatalytic performance of CuO-CdO-BT was evaluated for the degradation antibiotic levofloxacin (LVF) under natural sunlight. All experiments were performed on sunny days with radiation intensity of ~270 Klux in August and September 2021 from 12 noon to 2 p.m. at latitude 32.8621 and longitude

59.193995. Typically, the CuO-CdO-BT (0.4 g/L) were added into 50 mL of LVF solution (10 ppm). Prior irradiation, to reach adsorption–desorption equilibrium, the reaction samples were stirred in the darkness conditions for 30 minutes at laboratory temperature. Subsequently, the light reaction was performed under sunlight with an average intensity of 280 Klux. At predetermined time intervals, 3 mL suspension was separated using filter paper to remove the CuO-CdO-BT. The relevant concentration of residual LVF was measured using an UV–Vis spectrophotometer at 288 nm using the related calibration plot. The degradation efficiency of LVF was calculated as below:

$$\text{Degradation efficiency (\%)} = \frac{(C_0 - C)}{C_0} \times 100$$

Where, C_0 and C denote the initial concentration and LVF concentration (mg/L) at time t (min).

3. Results And Discussions

3.1 Synthesis of CuO-CdO-BT heterojunction

In the present study, the CuO-CdO-BT is synthesized *via* a green route in the presence of the aqueous extract of *Ferula* without the using any toxic chemicals and hazardous organic solvent. In this environmentally-friendly process, the *Ferula* effectively acts as a green reducing and capping agent for the synthesis of CdO and CuO NPs. A schematic representation of the synthesis of CuO-CdO-BT is exhibited in Fig. 1. The phenolic compounds in *Ferula* contributed to the bio-reduction of the Cu^{2+} and Cd^{2+} ions to Cu and Cd NPs, respectively[32, 33]. Finally, CdO and CuO NPs are obtained after calcination in a furnace at 500°C for 2 h.

3.2. Characterizations

FTIR analysis is carried out to study the functional group of compounds. The FTIR spectra of CuO-CdO-BT, bentonite, CuO NPs and CdO NPs are displayed in Fig. 2a. In all spectra, a broad peak at 3414 cm^{-1} is observed, which is attributed to O-H stretching vibrations[34]. Also, the spectral peak at about 1620 cm^{-1} is related to the H-OH bending vibrations. In FT-IR spectra of bentonite and CuO-CdO-BT, the absorption band at 3626 cm^{-1} is corresponded to in-plane O-H stretching vibrations of Si/Al-OH in the structure of bentonite[35]. The strong band located at 1033 cm^{-1} is correlated to the stretching vibrations of Si-O functional groups[36]. Also, the absorption band at about 470 cm^{-1} is related to Si-O-Si and Si-Al-O bending vibrations in structure of bentonite [37]. Two bands at 543 and 532 cm^{-1} are the characteristic bands of metal oxide Cd–O and Cu-O bonding, respectively[38, 39]. As shown in Fig. 2a, the absorption bands of the functional groups are observed without any special shift in the structure of biosynthesized nanocomposite.

Comparative crystal structure and phase purities of raw bentonite, CuO-CdO-BT and biosynthesized CdO and CuO NPs are determined by using XRD patterns (Fig. 2b). The diffraction peaks for CdO NPs are seen

at 2θ = 33.09° (1 1 1), 38.39° (2 0 0), 55.37° (2 2 0), 66.14° (3 1 1) and 69.75° (2 2 2) which are indexed to the crystal structure cadmium oxide (JCPDS No. 075–0593)[40]. In XRD pattern of CuO NPs, the peaks at 2θ values of 32.54◦, 35.61◦, 38.75◦, 48.84◦, 54.02◦, 58.46◦, 61.74◦, 66.44◦, 68.37◦, 72.86◦ and 75.70◦ corresponded to the (-1 1 0), (0 0 2), (1 1 1), (-2 0 2), (0 2 0), (2 0 2), (-1 1 3), (-3 1 1), (-2 2 0), (3 1 1) and (-2 2 2) planes of monoclinic copper oxide, respectively (JCPDS No. 45–0937)[30]. The raw bentonite contains constituents such as quartz (JCPDS No 083–0539)[41], albite (JCPDS No 001-0739)[42], and montmorillonite (JCPDS No 002–0037)[43]. The diffraction peak at 26.66◦ (1 0 1) is consistent with the characteristic peaks of quartz. The peaks at 2θ = 21.92° and 27.80° correspond to (-2 0 1) and (0 0 2) planes of albite. The presence of montmorillonite is also indicated by the located peaks at 2θ = 7.16° (0 0 1), 19.90° (1 1 0), 29.52 (1 1 3), 35.39° (1 0 4), 54.01 (1 4 4) and 62.35° (0 6 1). After the anchoring of CuO and CdO NPs on support, not only is the crystalline structure of bentonite retained, but also the diffraction peaks of CuO NPs, CdO NPs and bentonite is observed in XRD pattern of CuO-CdO-BT. The obtained results are confirmed the successful fabrication of CuO-CdO-BT.

The morphology of raw bentonite, CuO NPs, CdO NPs and CuO-CdO-BT is identified using field emission scanning electron microscopy (FE-SEM). As shown in the Fig. 3a, the raw bentonite shows the irregular sheet-like structure. The thickness of the layers in bentonite is about 19 nm. Fig.s 3b and 3c reveals FE-SEM of the bare CuO NPs and CdO NPs. After anchoring of nanoparticles on bentonite, the layered configuration of bentonite is somewhat preserved and the uniform dispersion of CuO and CdO NPs on the bentonite layers is also well seen. As shown Fig. 3d, the use of bentonite as a support not only reduces the agglomeration of CuO and CdO NPs, but also decreases the size of biosynthesized NPs, which in turn increases the active surface of NPs and enhances the adsorption of pollutant molecules[44]. Further, the presence of CuO and CdO NPs on the surface of bentonite is confirmed by elemental mapping and EDX analysis. EDX analysis clearly indicates that CuO-CdO-BT contains O (48.37 wt%), Fe (23.39 wt%), Si (12.84 wt%), Al (5.52 wt%), Ca (2.81 wt%), Mg (0.82 wt%), Na (0.37 wt%), Cd (3.47%) and Cu (2.41 wt%) elements (Fig. 3e). Fe, Si, Al, Ca, Mg and Na elements are associated with bentonite platform whereas Cd and Cu elements are originated from decorated CuO and CdO NPs. O element is also present in both the bentonite and nanoparticles. The elemental mapping shows the distribution of elements in nanocomposite (Fig. 3f). This proves the successful synthesis of biosynthesized CuO-CdO-BT.

The surface elemental compositions and valence state of CuO-CdO-BT are studied by XPS. Binding energy of C1s peak at 285.5 eV is applied as an internal calibration standard. As shown in Fig. 3g, the survey XPS spectrum of CuO-CdO-BT indicates the presence of Fe, O, Ca, Si, Al Cu and Cd elements which are the main components of bentonite, CuO and CdO NPs, respectively. To more information on oxidation states of Cu, Cd and O elements, the Cu2p, Cd3d and O1s are performed in high resolution (Fig. 3h-j). Two peaks at 933.00 and 953.93 eV attributed to the $Cu2p_{1/2}$ and $Cu2p_{3/2}$, which correspond to the typical Cu^{2+} valance state in CuO[7]. Also, the XPS spectrum shows two peaks at 403.41 and 411.04 eV characteristic for Cd $2d_{3/2}$ and $2d_{5/2}$ which are attributed to 2+ oxidation state of cadmium in the form of CdO. The peak attributed to O^{2-} is exhibited at 532.24 eV which corresponds to O1s[45].

Consequently, the combination of XRD, Fe-SEM, EDX, elemental mapping and XPS results confirms that the bentonite surface is sucssefully decorated with CuO and CdO NPs.

N_2 adsorption–desorption isotherms of bentonite and CuO-CdO-BT are displayed in Fig. S1. As shown, isotherms are type IV with a H3-type hysteresis hoop, indicating that the samples possess layered mesoporous structure[46]. The surface structure characteristics of bentonite and CuO-CdO-BT are summarized in Table S1. The BET results demonstrate that the specific surface area of CuO-CdO-BT is almost twice that of bentonite. These increases can be due to the intercalation of nanoparticles into/on the bentonite interlayers[47]. The high specific surface area of CuO-CdO-BT enables the possibility of efficient transfer of electrons and ions, leading to the better photocatalytic activity of nanocomposite. In addition, larger specific surface and pore volume lead to better interaction between CuO-CdO-BT and contaminant molecules.

The photo-absorption behavior of the biosynthesized is studied by UV–vis DRS. As displayed in Fig. S2a, the measured absorption edges of the CuO NPs and CdO NPs are 383 and 501 nm. Fig. S2b presents the Tauc's plot of samples which is in step with the Kubelka–Munk equation, i.e. $\alpha h\upsilon = A(h\upsilon - E_g)^n$ where, A is the absorption constant, $h\upsilon$ is the photon energy, $\mathrm{E_g}$ is the energy band gap and n is 1/2 or 2 for direct or indirect optical transition, respectively[48]. The direct band gap energy of pure CuO NPs and CdO NPs are found as 3.20 and 2.47 eV, respectively. The these results are similar to the findings in the literature[12, 45]. Amazingly, contrasted with bare CuO NPs and CdO NPs, the edge of absorption of CuO-CdO-BT reveals distinct red-shift and the band gap energy of nanocomposite is obtained about 1.87 eV. The decrease in band gap value of CuO-CdO-BT may be due to the defects in the crystal system[49]. Therefore, it can be concluded that the presence of bentonite and CuO/CdO heterojunction reduce the energy of the band gap and consequently increase the photocatalytic activity of the biosynthesized nanocomposite in the visible region[50].

3.3. Photocatalytic performance

LVF antibiotic is utilized as target pollutants to investigate the photocatalytic performance of the CuO-CdO-BT under sunlight. To obtain the optimal catalytic activity, the influences of the initial pH value, LVF concentration and dosage of photocatalyst on LVF degradation are investigated. The effect of solution pH on photocatalytic degradation of LVF using CuO-CdO-BT is examined at pHs 3 to 9. As shown in Fig. 4a, an increase in photodegradation of LVF is seen with increasing initial pH values up to 8. However, the difference in degradation efficiencies at pHs 7 and 8 was almost negligible. Then, with further increase in pH, the LVF removal efficiency is decreased. It is important to note that when the pH < 5.85, LVF has cationic form and if the pH value > 8.39, LVF has anionic form. The zwitterionic form of LVF exists when pH value is in the range of 5.85–8.39[3]. Meanwhile, the point of zero charge ($\mathrm{pH_{pzc}}$) of CuO-CdO-BT is determined to be 5.3 using the zeta potential measurements (Fig. S3). This result indicates that charge surface of CuO-CdO-BT is positive at pH < 5.3, and is negative at pH > 5.3. It is concluded that the decreasing in degradation at low pH values is due to electrostatic repulsions between the positively charged CuO-CdO-BT and LVF, which reduces the synergy of adsorption and photocatalytic

activity. Further degradation of LVF in relatively alkaline conditions compared to neutral or acidic conditions may be due to the better formation of $^{\bullet}OH$ and $O_2^{\bullet -}$ radicals, which ultimately improves the degradation process. As a result, the best LVF degradation efficiency is obtained 96.11% at pH 8.

In real environments, the concentration of LVF is very variable. Therefore, it is necessary to investigate the effect of different initial concentrations of LVF on photocatalytic performance. As shown Fig. 4b, the photodegradation efficiency of LVF is decreased from 96.11–24.95% as the LVF concentration increases from 10 to 100 mg/L. In fact, the generated intermediates in higher concentration of LVF are the main competitors of LVF molecules for contact with photocatalyst. In addition, high initial concentrations of LVF can limit the penetration of light into the solution and prevent photons from reaching the photocatalyst surface. So, the LVF concentration is selected as 10 mg/L in remaining tests to achieve the best photocatalytic activity.

The catalysts dose is an important factor in reducing industrial production costs and achieving high efficiency. The photocatalytic performance of CuO-CdO-BT in LVF degradation is investigated by changing the catalyst dose from 0.4 to 0.02 g/L to find the optimal dose. As displayed in Fig. 4c, the degradation of LVF is decreased from 96.11–41.46% with decreasing in the amount of catalyst from 0.4 to 0.02 g/L. However, the low degradation efficiency at low doses of CuO-CdO-BT can be attributed to lim ited active sites on the photocatalyst surface, which leads to reduced production of active species[52].

The photocatalytic degradation of LVF is studied in the absence and in the presence of metal oxides forming the CuO-CdO-BT nano-heterojunction under the optimal conditions (catalyst dosage: 0.4 g/L, LVF concentration: 10 mg/L and pH: 8). Any degradation of LVF is not observed in the absence of CuO-CdO-BT under sunlight after 30 min. The photodegradation yield of LVF is obtained 96.11%, 74.54% and 53.69% using CuO-CdO-BT, bare CuO NPs and CdO NPs, respectively (Fig. 4d). For better understanding the difference in the degradation performance using different catalysts, kinetic study for photodegradation of LVF is evaluated as the equation for pseudo-first-order kinetic model[53]:

$$-\ln\left(\frac{C}{C_0}\right) = k_{obs}t$$

Where k_{obs} is the first-order rate constant (min^{-1}), C_0 and C are the initial concentration and LVF concentration (mg/L) at time t (min), respectively. As presented in Fig. 4e, k_{obs} is calculated to be 0.108225, 0.045626 and 0.025666 min^{-1} for CuO-CdO-BT, CuO NPs and CdO NPs, respectively. The degradation of LVF using CuO-CdO-BT is about 2.4 and 4.2 times higher than bare CuO NPs and CdO NPs, respectively. The obtained results reveals that CuO-CdO-BT has much better photocatalytic performance than individual components, which can be related to fast electron-hole recombination and high aggregation of bare nanoparticles[44]. Also, since the correlation coefficient (R^2) is higher than 0.96 for all samples, it is inferred that the experimental data of LVF degradation by all studied processes are in

good agreement with the pseudo-first-order kinetic model[54]. To better evaluate the effectiveness of the CuO-CdO-BT, the synergy index is also calculated using the following equation:

$$\text{Synergyindex} = \frac{k_{obs\,(\,CuO-\,CdO-\,BT)}}{k_{obs\,(\,CuO)} + k_{obs\,(\,CdO)}}$$

The synergy index is calculated at 1.518. Due to the fact that the synergy index more than 1 has positive effect on the coupling of semiconductors, so this heterojunction is able to perform LVF degradation better than any of the nanoparticles alone. A detailed discussion of the reasons for this increase is provided in the section of charge transfer process.

In real water, there are some anions that can interfere with the removal of contaminants. Investigating the effect of the presence of anions on IVF degradation can provide a theoretical basis for industrial applications. Here, the typical anions (1 mM) such as sulfate (SO_4^{2-}), bicarbonate (HCO_3^-), nitrate (NO_3^-) and chloride (Cl^-) are added into the system to study their influence on the LVF degradation. As displayed in Fig. 5a, the presence of SO_4^{2-}, HCO_3^-, and NO_3^- anions cause negligible effect on the degradation process. SO_4^-, HCO_3^- andNO_3^- radicals are more selective than $^-$OH radicals because of their large structure, so they are less likely to react with LVF. The presence of Cl^- anion leads to a slight decrease in the photodegradation process, which probably results from the inevitable competitive adsorption between Cl^- and LVF molecules at the active sites of CuO-CdO-BT[51].

In the following, the radical quenching experiments are performed to find the predominant contribution of each reactive species in LVF degradation process. Benzoquinone (BQ), isopropyl alcohol (IPA) and ammonium oxalate (AO) are utilized as the quenching agents to determine the role of $O_2^{\bullet -}$ and $^{\cdot}$OH radicals and h^+, respectively[55]. As exhibited in Fig. 5b, although all reactive species participated in the photodegradation of LVF, the degradation performance of LVF is clearly quenched using BQ and IPA which illustrated that $^{\cdot}$OHand $O_2^{\bullet -}$ radicals are main active species in the photodegradation of LVF using CuO-CdO-BT under sunlight.

To verify S-scheme charge transfer process in the CuO-CdO-BT heterojunction, at first, the conduction bond (E_{CB}) and valance bond (E_{VB}) energies of CuO NPs and CdO NPs are determined according to the Mulliken electronegativity equations[56]:

$$E_{CB} = \chi - E_C - 0.5E_g$$

E_{VB} = E_{CB} + E_g

Where, E_C is the energy of free electrons (~ 4.5 eV) on the hydrogen scale. The values of χ (absolute electronegativity) for CuO and CdO NPs are 5.81 and 4.67 eV, respectively [57, 58]. The E_g values of CuO (3.2 eV) and CdO (2.47 eV) are obtained by DRS analysis, therefore, the calculated E_{CB} and E_{VB} values

are to be -0.29 and 2.91 eV for CuO NPs and -1.06 and 1.40 eV for CdO NPs, respectively. A band diagram of CuO-CdO-BT is given in three modes: before contact, after contact and after being exposed to sunlight (Fig. 6). If CuO or CdO NPs were used alone, an undesirable recombination of electron-hole pairs would occur rapidly, ultimately reducing photocatalytic activity. Fortunately, in the present case, this problem has been solved by using the S-scheme heterojunction through the efficient separation of photogenerated charge transporters[16]. As shown in Fig. 6, since CdO NPs have higher $\mathrm{E_{CB}}$ and $\mathrm{E_{VB}}$ than those CuO NPs, when CdO and CuO NPs are in close contact, the electrons are transferred from CdO to CuO spontaneously across their interface. The electron transfer causes CdO to be positive and CuO to be negative at interface of two semiconductors[59]. As a result, an internal electric field (IEF) is formed directing from CdO to CuO. IEF leads to the energy band edge of CdO and CuO bend upward and downward toward the interface, respectively[60]. The band bending causes electrons in the VB of CdO and holes in the CB of CuO at the interface region to be recombined. Thus, under sunlight, the useless electrons and holes are removed from the photocatalytic system *via* recombination, in the event that the useful electrons and holes are retained in the CB of CdO and VB of CuO, respectively. The electrons and holes at more suitable redox potentials react with O_2 and H_2O to generate $\mathrm{O_2^{\bullet -}}$ and $^{\cdot}$OHradicals, respectively[61]. Finally, the charge carriers and radicals degrade LVF into simple harmless molecules.

In order to study the pathways of LVF degradation, HPLC-MS analysis is performed and according to the comparative analysis of the obtained results with related literature[62, 63], six possible pathways of LVF degradation are suggested (Scheme 1). The chromatograms of the identified degradation intermediates after 15 min and 30 min are exhibited in Fig. S5. In pathway I, the oxidation of piperazine ring is occurred and produced P1 that is further oxidized into P2, P3 and P4. P5 is formed *via* decarboxylation. Also, P6 is generated through the removal of fluorine group and the cleavage carbon-nitrogen bond on the residue of the piperazine ring. Pathway II starts with decarboxylation of the quinolone ring and P7 is produced. Subsequently, the piperazine ring is separated and only its amine group remains, thus forming the P8. When this amine group is also separated, P9 is generated. In parallel, P7 can be transformed into P10 *via* defluorination. Also, P11 is produced by releasing the fluorine, methyl and hydrogen groups from P7. In pathway III, the fluorine group is displaced by a hydroxyl group to generate P12. Then, P13, P14 and P15 are formed through the oxidation and decarbonylation of piperazin. The quinolone ring can be opened by reactive oxygen species to produce P17 and P18. Also, P19 is generated by demethylation of the piperazine ring. In pathway IV, initially, the LVF is oxidized *via* carboxylation, resulting in the formation of P19. Then, P20 is produced by removing the methyl group from piperazine, followed by the ring opening process to become P21. Eventually, P22 is obtained following decarboxylation, depiperazinylation and the ring opening of benzene group process. Pathway V begins with demethylation of LVF to generate P23. Then, P25 is produced by decarboxylation, defluorination, and hydroxylation. In pathway VI, P26 is obtained by defluorination and piperazine ring opening of LVF. Then, P27 is produced *via* decarboxylation. P27 is further oxidized by cleaving the carbon-nitrogen bond, followed by decarbonylation to form P28. As displayed in Fig. S1, LVF is effectively degraded using CuO-CdO-BT because the related peak to LVF (m/z = 362) is disappeared and the intermediate peaks with lower mass appeared after 30 minutes.

The catalyst stability study is carried out using CuO-CdO-BT with fresh LVF solution under sunlight in three consecutive cycles. After each cycle is finished, the photocatalyst is separated by centrifugation and after washing and drying, it is used again in the experiment under the same conditions. As shown in Fig. S4, the photodegradation efficiency of CuO-CdO-BT is slightly decreased after three cycles of photodegradation as compared to the first cycle. Based on these experiments, it can be concluded that CuO-CdO-BT has high stability and recyclability.

In order to demonstrate the higher degradation of LVF using CuO-CdO-BT than other photocatalysts, the results of this study are compared with some previous reports in Table 1. As shown Table 1, CuO-CdO-BT presented relatively higher performance for LVF photodegradation in a shorter time without any auxiliary agent.

Table 1
Comparison of the removal efficiency of LVF in various systems

Catalyst	LVF concentration (mg/L)	Catalyst dosage (g/L)	Time (min)	Photocatalyst synthesis method	Efficiency (%)
CuO-CdO-BT	10	0.4	30	green	96.11[this study]
$(BiOBr)x(Bi_7O_9I_3)_{1-x}$	50	1	120	solvothermal	95.4[64]
BiOCl/BiOBr–$Bi_{24}O_{31}Br_{10}$	50	1	180	solvothermal	80.2[65]
α-Bi_2O_3/C-dots	10	1	120	sonochemical	79[66]
g-C_3N_4/MoS_2	10	1	140	hydrothermal	75.81[67]
$BaZrO_3$/W	10	0.2	180	hydrothermal	93.4[3]
Ta_3N_5/TiO_2	10	1	120	hydrothermal	92.8[68]
Ag_2O/$Bi_{12}GeO_2$	10	0.5	120	hydrothermal	~ 72[69]
Au/h-BN	10	1	210	wet impregnation	84.4[70]
CdS/$Bi_{12}GeO_{20}$	10	0.5	120	hydrothermal	80[71]
rGO-CdS	10	0.5	60	hydrothermal	82.7[72]
Cu-TiO_2	50	1	360	micelle sol–gel	75[73]
Ag_3PO_4/GO/UiO − 66 − NH_2	25	0.8	60	sonochemical	94.97[74]
CFC/UiO-66-NH_2/AgI	10	It was not mentioned	120	chemical deposition	84.5[75]

Conclusion

In this paper, to meliorate the photocatalytic efficiency, a novel S-scheme heterojunction photocatalyst was synthesized using plant extract for the first time. In this regard, CuO and CdO NPs were synthesized using *Ferula* without any toxic reducing agent and surfactant and anchored on layered bentonite (denoted as CuO-CdO-BT). The physicochemical features of biosynthesized photocatalyst were verified using various characterization techniques including FT-IR, XRD, FE-SEM, elemental mapping, EDX, XPS, N_2 adsorption–desorption and UV–vis DRS analyzes. The photocatalytic activity of CuO-CdO-BT for the photodegradation of LVF was investigated under natural sunlight. The advanced sunlight-driven catalytic performance benefited from the unique structure of CuO-CdO-BT. As anticipated, the interfacial defect

between two CuO and CdO semiconductors in the coupled system creates favorable conditions for the fast charges transfer, separation of photogenerated electron-hole pairs and the capture of sunlight. The best reaction conditions were as follows: the reaction pH value was 8, the amount of LVF was 10 mg/L and catalysts dose was 0.4 g/L. The LVF photodegradation was obtained 96.11% which was much higher than that of most reported photocatalysts. As Quenching tests, although all reactive species participated in the photodegradation of LVF, the contribution of $O_2^{\bullet -}$ and $^{\cdot}OH$ radicals is more pronounced in CuO-CdO-BT system. The anions had little effect on degradation, however, among the considered interfering ions, Cl^- displayed the most inhibitory effect on LVF degradation. More than 88.5% levofloxacin was degraded by the system after three cycles of photodegradation, suggesting a cost-effectiveness potential in the recyclability of CuO-CdO-BT. The photodegradation in the presence of natural sunlight as a renewable energy and affordable source is one of advantages of this method. The present work will open a novel gateway for the construction of biologically and environmentally inspired photocatalysts for effective removal of pharmaceutical contaminants and will support the slogan of achieving a clean land for the future generation.

Declarations

Acknowledgments

The authors highly appreciated of the University of Birjand and Birjand University of Technology for supporting this study.

Author contribution

All authors contributed to the study conception and design. Majid Mahjoore: Formal analysis, Methodology, Data Curation, Moones Honarmand: Supervision, Writing - Review & Editing, Visualization, Investigation, Ahmad Aryafar: Project administration, Supervision, Conceptualization, Resources

Funding: No funding has been received by any organizations.

Conflict of interest: The authors declare no competing interests.

References

1. Fedorowicz J, Sączewski J (2018) Modifications of quinolones and fluoroquinolones: hybrid compounds and dual-action molecules. Monatshefte für Chemie - Chem Mon 149:1199–1245. https://doi.org/10.1007/s00706-018-2215-x
2. Meng F, Wang Y, Chen Z, Hu J, Lu G, Ma W (2021) Synthesis of CQDs@FeOOH nanoneedles with abundant active edges for efficient electro-catalytic degradation of levofloxacin: Degradation mechanism and toxicity assessment. Appl Catal B Environ 282:119597–119609. https://doi.org/10.1016/j.apcatb.2020.119597

3. Gulen B, Demircivi P, Simsek EB (2021) UV-A light irradiated photocatalytic performance of hydrothermally obtained W doped $BaZrO_3$ catalyst against the degradation of levofloxacin and tetracycline antibiotic. J Photochem Photobiol A Chem 404:112869–112877. https://doi.org/10.1016/j.jphotochem.2020.112869
4. Hassani A, Eghbali P, Kakavandi B, Lin KYA, Ghanbari F (2020) Acetaminophen removal from aqueous solutions through peroxymonosulfate activation by $CoFe_2O_4$/mpg-C_3N_4 nanocomposite: Insight into the performance and degradation kinetics. Environ Technol Innov 20:101127–101140. https://doi.org/10.1016/j.eti.2020.101127
5. Sekar P, Sadanand Joshi D, Manjunatha M, Mahalingam H (2022) Enhanced disinfection of E. faecalis and levofloxacin antibiotic degradation using tridoped B-Ce-Ag TiO_2 photocatalysts synthesized by ecofriendly citrate EDTA complexing method. Environ Sci Pollut Res 50765–50779. https://doi.org/10.1007/s11356-022-19268-x
6. Zhang Y, Zheng J, Nan J, Gai C, Shao Q, Murugadoss V, Maganti S, Naik N, Algadi H, Huang M, Xu B Bin, Guo Z (2022) Influence of mass ratio and calcination temperature on physical and photoelectrochemical properties of ZnFe-layered double oxide/cobalt oxide heterojunction semiconductor for dye degradation applications. Particuology 74:141–155. https://doi.org/10.1016/j.partic.2022.05.010
7. Moradi M, Hasanvandian F, Isari AA, Hayati F, Kakavandi B, Setayesh SR (2021) CuO and ZnO co-anchored on g-C_3N_4 nanosheets as an affordable double Z-scheme nanocomposite for photocatalytic decontamination of amoxicillin. Appl Catal B Environ 285:119838–119853. https://doi.org/10.1016/j.apcatb.2020.119838
8. Zhang Y, Shao Q, Jiang H, Liu L, Wu M, Lin J, Zhang J, Wu S, Dong M, Guo Z (2020) One-step co-precipitation synthesis of novel BiOCl/CeO_2 composites with enhanced photodegradation of rhodamine B. Inorg Chem Front 7:1345–1361. https://doi.org/10.1039/c9qi01524h
9. Sun P, Zhou S, Yang Y, Liu S, Cao Q, Wang Y, Wågberg T, Hu G (2022) Artificial chloroplast-like phosphotungstic acid — iron oxide microbox heterojunctions penetrated by carbon nanotubes for solar photocatalytic degradation of tetracycline antibiotics in wastewater. Adv Compos Hybrid Mater. https://doi.org/10.1007/s42114-022-00462-x
10. Ighalo JO, Sagboye PA, Umenweke G, Ajala OJ, Omoarukhe FO, Adeyanju CA, Ogunniyi S, Adeniyi AG (2021) CuO nanoparticles (CuO NPs) for water treatment: A review of recent advances. Environ Nanotechnology, Monit Manag 15:100443–100454. https://doi.org/10.1016/j.enmm.2021.100443
11. Dror I, Fink L, Weiner L, Berkowitz B (2020) Elucidating the catalytic degradation of enrofloxacin by copper oxide nanoparticles through the identification of the reactive oxygen species. Chemosphere 258:127266–127272
12. Muthuvel A, Jothibas M, Manoharan C (2020) Synthesis of copper oxide nanoparticles by chemical and biogenic methods: photocatalytic degradation and in vitro antioxidant activity. Nanotechnol Environ Eng 5:14–32. https://doi.org/10.1007/s41204-020-00078-w

13. Chamanehpour E, Sayadi MH, Hajiani M (2022) A hierarchical graphitic carbon nitride supported by metal–organic framework and copper nanocomposite as a novel bifunctional catalyst with long-term stability for enhanced carbon dioxide photoreduction under solar light irradiation. Adv Compos Hybrid Mater. https://doi.org/10.1007/s42114-022-00459-6
14. Zheng J, Zhang Y, Jing C, Zhang H, Shao Q, Ge R (2022) A visible-light active p-n heterojunction ZnO/Co_3O_4 composites supported on Ni foam as photoanode for enhanced photoelectrocatalytic removal of methylene blue. Adv Compos Hybrid Mater. https://doi.org/10.1007/s42114-022-00448-9
15. Fu J, Xu Q, Low J, Jiang C, Yu J (2019) Ultrathin 2D/2D WO_3/g-C_3N_4 step-scheme H_2-production photocatalyst. Appl Catal B Environ 243:556–565. https://doi.org/10.1016/j.apcatb.2018.11.011
16. Xu Q, Zhang L, Cheng B, Fan J, Yu J (2020) S-Scheme Heterojunction Photocatalyst. Chem 6:1543–1559. https://doi.org/10.1016/j.chempr.2020.06.010
17. Hamad H, Elsenety MM, Sadik W, El-Demerdash A-G, Nashed A, Mostafa A, Elyamny S (2022) The superior photocatalytic performance and DFT insights of S-scheme CuO@TiO_2 heterojunction composites for simultaneous degradation of organics. Sci Rep 12:2217–2236. https://doi.org/10.1038/s41598-022-05981-7
18. Munawar T, Yasmeen S, Hussain F, Mahmood K, Hussain A, Asghar M, Iqbal F (2020) Synthesis of novel heterostructured ZnO-CdO-CuO nanocomposite: Characterization and enhanced sunlight driven photocatalytic activity. Mater Chem Phys 249:122983–122994. https://doi.org/10.1016/j.matchemphys.2020.122983
19. Das T, Chatterjee R, Majee A, Uyama H, Morgan D, Nandi M (2019) In situ synthesis of CuO nanoparticles over functionalized mesoporous silica and their application in catalytic syntheses of symmetrical diselenides. Dalt Trans 48:17874–17886. https://doi.org/10.1039/c9dt03418h
20. Gholamali I, Alipour E (2020) Carboxymethyl Chitosan/Starch/CuO Nanocomposite Hydrogels for Controlled Release of Amoxicillin. Regen Eng Transl Med 6:398–406. https://doi.org/10.1007/s40883-020-00173-z
21. Saberi A, Alipour E, Sadeghi M (2019) Superabsorbent magnetic Fe_3O_4-based starch-poly (acrylic acid) nanocomposite hydrogel for efficient removal of dyes and heavy metal ions from water. J Polym Res 26:271–284. https://doi.org/10.1007/s10965-019-1917-z
22. Mirzaei D, Zabardasti A, Mansourpanah Y, Sadeghi M, Farhadi S (2020) Efficacy of Novel NaX/MgO–TiO_2 Zeolite Nanocomposite for the Adsorption of Methyl Orange (MO) Dye: Isotherm, Kinetic and Thermodynamic Studies. J Inorg Organomet Polym Mater 30:2067–2080. https://doi.org/10.1007/s10904-019-01369-9
23. Ramin M, Taleshi F (2013) The effect of carbon nanotubes as a support on morphology and size of silver nanoparticles. Int Nano Lett 3:1–6. https://doi.org/10.1186/2228-5326-3-32
24. Singh N, Jana S, Singh GP, Dey RK (2020) Graphene-supported TiO_2: study of promotion of charge carrier in photocatalytic water splitting and methylene blue dye degradation. Adv Compos Hybrid Mater 3:127–140. https://doi.org/10.1007/s42114-020-00140-w

25. Yu M, Yu T, Chen S, Guo Z, Seok I (2020) A Facile Synthesis of Ag/TiO_2/rGO Nanocomposites with Enhanced Visible Light Photocatalytic Activity. ES Mater Manuf 7:64–69. https://doi.org/10.30919/esmm5f712
26. Honarmand M, Golmohammadi M, Naeimi A (2020) Green synthesis of SnO_2-bentonite nanocomposites for the efficient photodegradation of methylene blue and eriochrome black-T. Mater Chem Phys 241:122416–122426. https://doi.org/10.1016/j.matchemphys.2019.122416
27. Mishra A, Mehta A, Kainth S, Basu S (2018) A comparative study on the effect of different precursors for synthesis and efficient photocatalytic activity of g-C_3N_4/TiO_2/bentonite nanocomposites. J Mater Sci 53:13126–13142. https://doi.org/10.1007/s10853-018-2565-0
28. Naeimi A, Honarmand M, Ali Chaji M, Khosravi S (2022) Green synthesis of bentonite/cellulose@lead oxide bio-nanocomposite with assistance of Pistacia Atlantica extract for efficient photocatalytic degradation of ciprofloxacin. Adv Powder Technol 33:103441–103452. https://doi.org/10.1016/j.apt.2022.103441
29. Baig N, Kammakakam I, Falath W, Kammakakam I (2021) Nanomaterials: A review of synthesis methods, properties, recent progress, and challenges. Mater Adv 2:1821–1871. https://doi.org/10.1039/d0ma00807a
30. Sharma JK, Akhtar MS, Ameen S, Srivastava P, Singh G (2015) Green synthesis of CuO nanoparticles with leaf extract of Calotropis gigantea and its dye-sensitized solar cells applications. J Alloys Compd 632:321–325. https://doi.org/10.1016/j.jallcom.2015.01.172
31. Ghotekar S (2017) Green Synthesis of Fluorescent CdO Nanoparticles using Leucaena leucocephala L. Extract and their Biological Activities. J Bacteriol Mycol Open Access 5:373–376. https://doi.org/10.15406/jbmoa.2017.05.00148
32. Hosseinzadeh N, Shomali T, Hosseinzadeh S, Raouf Fard F, Pourmontaseri M, Fazeli M (2020) Green synthesis of gold nanoparticles by using Ferula persica Willd. gum essential oil: production, characterization and in vitro anti-cancer effects. J Pharm Pharmacol 72:1013–1025. https://doi.org/10.1111/jphp.13274
33. Hashemi Z, Mohammadyan M, Naderi S, Fakhar M, Biparva P, Akhtari J, Ebrahimzadeh MA (2021) Green synthesis of silver nanoparticles using Ferula persica extract (Fp-NPs): Characterization, antibacterial, antileishmanial, and in vitro anticancer activities. Mater Today Commun 27:102264–102273. https://doi.org/10.1016/j.mtcomm.2021.102264
34. Golmohammadi M, Honarmand M, Esmaeili A (2022) Biosynthesis of ZnO nanoparticles supported on bentonite and the evaluation of its photocatalytic activity. Mater Res Bull 149:111714–111723. https://doi.org/10.1016/j.materresbull.2021.111714
35. Kaur M, Ubhi MK, Singh D (2018) Magnetically retrievable nanocomposite of magnesium ferrite and bentonite clay for sequestration of Pb(II) and Ni(II) ions: A comparative study. Bull Mater Sci 41:132–145. https://doi.org/10.1007/s12034-018-1647-6
36. Shah KH, Ali S, Waseem M, Shah F, Fahad M, Shahida S, Khan AM, Khan AR (2019) Native and Magnetic Oxide Nanoparticles (Fe_3O_4) Impregnated Bentonite Clays as Economic Adsorbents for

Cr(III) Removal. J Solution Chem 48:1640–1656. https://doi.org/10.1007/s10953-019-00912-z

37. Amulya MAS, Nagaswarupa HP, Kumar MRA, Ravikumar CR, Kusuma B (2021) Sonochemical synthesis of $MnFe_2O_4$ nanoparticles and their electrochemical and photocatalytic properties. J Phys Chem Solids 148:109661
38. Karthik K, Dhanuskodi S, Gobinath C, Prabukumar S, Sivaramakrishnan S (2017) Andrographis paniculata extract mediated green synthesis of CdO nanoparticles and its electrochemical and antibacterial studies. J Mater Sci Mater Electron 28:7991–8001. https://doi.org/10.1007/s10854-017-6503-8
39. Khalaji AD, Rohlicek J, Machek P, Das D (2014) A New Copper(I) Coordination Polymer with N2-Donor Schiff Base and Its Use as Precursor for CuO Nanoparticle: Spectroscopic, Thermal and Structural Studies. J Clust Sci 25:1425–1434. https://doi.org/10.1007/s10876-014-0719-z
40. Jeejamol DJ, Jayakumari K, Moses A, Raj E (2016) Outcome of Copper Incorporation in the Photocatalytic Activity of Cadmium Oxide Nanoparticles I Introduction. J Appl Sci Eng Methodol 2:356–362
41. Mobasherpour I, Javaherai M, Salahi E, Ebrahimi M, Ashrafı Z, Orooji Y (2021) Removal of pb(II) from aqueous solution by ceramsite prepared from isfahan bentonite and y-alumina. Chem Chem Technol 15:263–273. https://doi.org/10.23939/chcht15.02.263
42. Cótica LF, Freitas VF, Santos IA, Barabach M, Anaissi FJ, Miyahara RY, Sarvezuk PWC (2011) Cobalt-modified Brazilian bentonites: Preparation, characterisation, and thermal stability. Appl Clay Sci 51:187–191. https://doi.org/10.1016/j.clay.2010.10.033
43. Rosendo-González V, Illescas J, del Carmen Díaz-Nava M, Alvarado-Pérez Y, García-Sánchez JJ (2019) Synthesis and characterization of clay nanocomposites based on starch. MRS Adv 4:3243–3249. https://doi.org/10.1557/adv.2019.403
44. Caglar B, Guner EK, Ersoy S, Caglar S, Özdemir AO, Özdokur KV, Doğan B, İçer F, Çırak Ç (2021) Bi_2S_3 nanorods decorated on bentonite nanocomposite for enhanced visible-light-driven photocatalytic performance towards degradation of organic dyes. J Alloys Compd 885:160964–160980. https://doi.org/10.1016/j.jallcom.2021.160964
45. Nallendran R, Selvan G, Balu AR (2019) NiO coupled CdO nanoparticles with enhanced magnetic and antifungal properties. Surfaces and Interfaces 15:11–18. https://doi.org/10.1016/j.surfin.2019.02.002
46. Eslamipanah M, Jaleh B, Feizi Mohazzab B, Khazalpour S, Nasrollahzadeh M, Shokouhimehr M (2020) Facile synthesis and electrochemical hydrogen storage of bentonite/TiO_2/Au nanocomposite. Int J Hydrogen Energy 45:33771–33788. https://doi.org/10.1016/j.ijhydene.2020.09.044
47. Krishnan B, Mahalingam S (2017) Ag/TiO_2/bentonite nanocomposite for biological applications: Synthesis, characterization, antibacterial and cytotoxic investigations. Adv Powder Technol 28:2265–2280. https://doi.org/10.1016/j.apt.2017.06.007
48. Wu M, Jing T, Tian J, Qi H, Shi D, Zhao C, Chen T, Zhao Z, Zhang P, Guo Z (2022) Synergistic effect of silver plasmon resonance and p-n heterojunction enhanced photoelectrochemical aptasensing

platform for detecting chloramphenicol. Adv Compos Hybrid Mater. https://doi.org/10.1007/s42114-021-00377-z

49. Babu AT, Antony R (2019) Clay semiconductor hetero-system of SnO_2/bentonite nanocomposites for catalytic degradation of toxic organic wastes. Appl Clay Sci 183:105312–105321. https://doi.org/10.1016/j.clay.2019.105312
50. Ren B, Shen W, Li L, Wu S, Wang W (2018) 3D $CoFe_2O_4$ nanorod/flower-like MoS_2 nanosheet heterojunctions as recyclable visible light-driven photocatalysts for the degradation of organic dyes. Appl Surf Sci 447:711–723. https://doi.org/10.1016/j.apsusc.2018.04.064
51. Li L, Niu CG, Guo H, Wang J, Ruan M, Zhang L, Liang C, Liu HY, Yang YY (2020) Efficient degradation of Levofloxacin with magnetically separable $ZnFe_2O_4$/NCDs/Ag_2CO_3 Z-scheme heterojunction photocatalyst: Vis-NIR light response ability and mechanism insight. Chem Eng J 383:123192–123205. https://doi.org/10.1016/j.cej.2019.123192
52. Ain QU, Rasheed U, Yaseen M, Zhang H, Tong Z (2020) Superior dye degradation and adsorption capability of polydopamine modified Fe_3O_4-pillared bentonite composite. J Hazard Mater 397:122758. https://doi.org/10.1016/j.jhazmat.2020.122758
53. Nguyen LT, Nguyen HT, Pham TD, Tran TD, Chu HT, Dang HT, Nguyen VH, Nguyen KM, Pham TT, Van der Bruggen B (2020) UV–Visible Light Driven Photocatalytic Degradation of Ciprofloxacin by N,S Co-doped TiO_2: The Effect of Operational Parameters. Top Catal 63:985–995. https://doi.org/10.1007/s11244-020-01319-7
54. Mehrdoost A, Yengejeh RJ, Mohammadi MK, Haghighatzadeh A, Babaei AA (2022) Adsorption removal and photocatalytic degradation of azithromycin from aqueous solution using PAC/Fe/Ag/Zn nanocomposite. Environ Sci Pollut Res 29:33514–33527. https://doi.org/10.1007/s11356-021-18158-y
55. Prabavathi SL, Saravanakumar K, Park CM, Muthuraj V (2021) Photocatalytic degradation of levofloxacin by a novel Sm_6WO_{12}/g-C_3N_4 heterojunction: Performance, mechanism and degradation pathways. Sep Purif Technol 257:117985–117994. https://doi.org/10.1016/j.seppur.2020.117985
56. Moradi M, Kakavandi B, Bahadoran A, Giannakis S, Dehghanifard E (2022) Intensification of persulfate-mediated elimination of bisphenol A by a spinel cobalt ferrite-anchored g-C_3N_4 S-scheme photocatalyst: Catalytic synergies and mechanistic interpretation. Sep Purif Technol 285:120313–120330. https://doi.org/10.1016/j.seppur.2021.120313
57. Senobari S, Nezamzadeh-Ejhieh A (2020) A novel ternary nano-composite with a high photocatalyitic activity: Characterization, effect of calcination temperature and designing the experiments. J Photochem Photobiol A Chem 394:112455–112467. https://doi.org/10.1016/j.jphotochem.2020.112455
58. Husein DZ, Hassanien R, Khamis M (2021) Cadmium oxide nanoparticles/graphene composite: synthesis, theoretical insights into reactivity and adsorption study. RSC Adv 11:27027–27041. https://doi.org/10.1039/d1ra04754j

59. Deng H, Fei X, Yang Y, Fan J, Yu J, Cheng B, Zhang L (2021) S-scheme heterojunction based on p-type $ZnMn_2O_4$ and n-type ZnO with improved photocatalytic CO2 reduction activity. Chem Eng J 409:127377–127386. https://doi.org/10.1016/j.cej.2020.127377
60. Wu S, Yu X, Zhang J, Zhang Y, Zhu Y, Zhu M (2021) Construction of $BiOCl/CuBi_2O_4$ S-scheme heterojunction with oxygen vacancy for enhanced photocatalytic diclofenac degradation and nitric oxide removal. Chem Eng J 411:128555–128566. https://doi.org/10.1016/j.cej.2021.128555
61. Jia X, Han Q, Liu H, Li S, Bi H (2020) A dual strategy to construct flowerlike S-scheme $BiOBr/BiOAc_{1-x}Br_x$ heterojunction with enhanced visible-light photocatalytic activity. Chem Eng J 399:125701–125713. https://doi.org/10.1016/j.cej.2020.125701
62. Yang X, Xie X, Li S, Zhang W, Zhang X, Chai H, Huang Y (2021) The POM@MOF hybrid derived hierarchical hollow Mo/Co bimetal oxides nanocages for efficiently activating peroxymonosulfate to degrade levofloxacin. J Hazard Mater 419:126360–126361. https://doi.org/10.1016/j.jhazmat.2021.126360
63. Zhong X, Zhang KX, Wu D, Ye XY, Huang W, Zhou BX (2020) Enhanced photocatalytic degradation of levofloxacin by Fe-doped BiOCl nanosheets under LED light irradiation. Chem Eng J 383:123148. https://doi.org/10.1016/j.cej.2019.123148
64. Fard SG, Haghighi M, Shabani M (2019) Facile one-pot ultrasound-assisted solvothermal fabrication of ball-flowerlike nanostructured $(BiOBr)x(Bi_7O_9I_3)_{1-x}$ solid-solution for high active photodegradation of antibiotic levofloxacin under sun-light. Appl Catal B Environ 248:320–331. https://doi.org/10.1016/j.apcatb.2019.02.021
65. Heidari S, Haghighi M, Shabani M (2020) Sunlight-activated $BiOCl/BiOBr–Bi_{24}O_{31}Br_{10}$ photocatalyst for the removal of pharmaceutical compounds. J Clean Prod 259:120679. https://doi.org/10.1016/j.jclepro.2020.120679
66. Sharma S, Mehta SK, Ibhadon AO, Kansal SK (2019) Fabrication of novel carbon quantum dots modified bismuth oxide (α-Bi_2O_3/C-dots): Material properties and catalytic applications. J Colloid Interface Sci 533:227–237. https://doi.org/10.1016/j.jcis.2018.08.056
67. He Y, Ma Z, Junior LB (2020) Distinctive binary g-C_3N_4/MoS_2 heterojunctions with highly efficient ultrasonic catalytic degradation for levofloxacin and methylene blue. Ceram Int 46:12364–12372. https://doi.org/10.1016/j.ceramint.2020.01.287
68. Jiang Y, Jing X, Zhu K, Peng Z, Zhang J, Liu Y, Zhang W, Ni L, Liu Z (2018) Ta_3N_5 nanoparticles/TiO_2 hollow sphere (0D/3D) heterojunction: Facile synthesis and enhanced photocatalytic activities of levofloxacin degradation and H2 evolution. Dalt Trans 47:13113–13125. https://doi.org/10.1039/c8dt02343c
69. Ruan X, Hu H, Che H, Che G, Li C, Liu C, Dong H (2019) Facile fabrication of $Ag_2O/Bi_{12}GeO_{20}$ heterostructure with enhanced visible-light photocatalytic activity for the degradation of various antibiotics. J Alloys Compd 773:1089–1098. https://doi.org/10.1016/j.jallcom.2018.09.312

70. He Y, Xu N, Junior LB, Hao X, Yao B, Yang Q, Liu D, Ma Z (2020) Construction of AuNPs/h-BN nanocomposites by using gold as interfacial electron transfer mediator with highly efficient degradation for levofloxacin hydrochloride and hydrogen generation. Appl Surf Sci 520:146336–146347. https://doi.org/10.1016/j.apsusc.2020.146336
71. Ruan X, Hu H, Che H, Jiang E, Zhang X, Liu C, Che G (2019) A visible-light-driven Z-scheme CdS/$Bi_{12}GeO_{20}$ heterostructure with enhanced photocatalytic degradation of various organics and the reduction of aqueous Cr(VI). J Colloid Interface Sci 543:317–327. https://doi.org/10.1016/j.jcis.2019.02.052
72. Kaur M, Umar A, Mehta SK, Kansal SK (2019) Reduced graphene oxide-CdS heterostructure: An efficient fluorescent probe for the sensing of Ag(I) and sunset yellow and a visible-light responsive photocatalyst for the degradation of levofloxacin drug in aqueous phase. Appl Catal B Environ 245:143–158. https://doi.org/10.1016/j.apcatb.2018.12.042
73. Varma KS, Shukla AD, Tayade RJ, Joshi PA, Das AK, Modi KB, Gandhi VG (2022) Photocatalytic performance and interaction mechanism of reverse micelle synthesized Cu-TiO_2 nanomaterials towards levofloxacin under visible LED light. Photochem Photobiol Sci 21:77–89. https://doi.org/10.1007/s43630-021-00141-8
74. Zhu P, Lin J, Xie L, Duan M, Chen D, Luo D, Wu Y (2021) Visible Light Response Photocatalytic Performance of Z-Scheme Ag_3PO_4/GO/UiO-66-NH_2 Photocatalysts for the Levofloxacin Hydrochloride. Langmuir 37:13309–13321. https://doi.org/10.1021/acs.langmuir.1c01901
75. Qian T, Zhang Y, Cai J, Cao W, Liu T, Chen Z, Liu J, Li F, Zhang L (2021) Decoration of amine functionalized zirconium metal organic framework/silver iodide heterojunction on carbon fiber cloth as a filter- membrane-shaped photocatalyst for degrading antibiotics. J Colloid Interface Sci 603:582–593. https://doi.org/10.1016/j.jcis.2021.06.112

Scheme

Scheme 1 is available in Supplementary Files section.

Figures

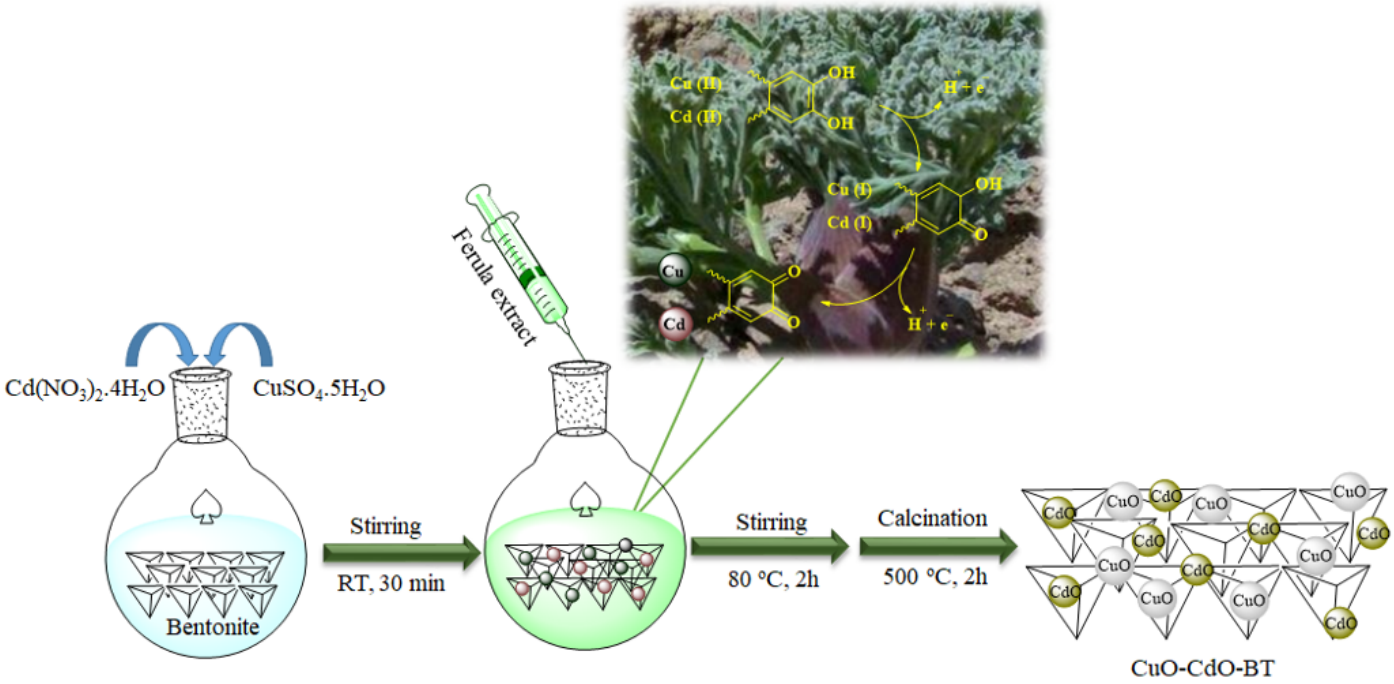


Figure 1

Schematic illustration of the green synthesis of CuO-CdO-BT

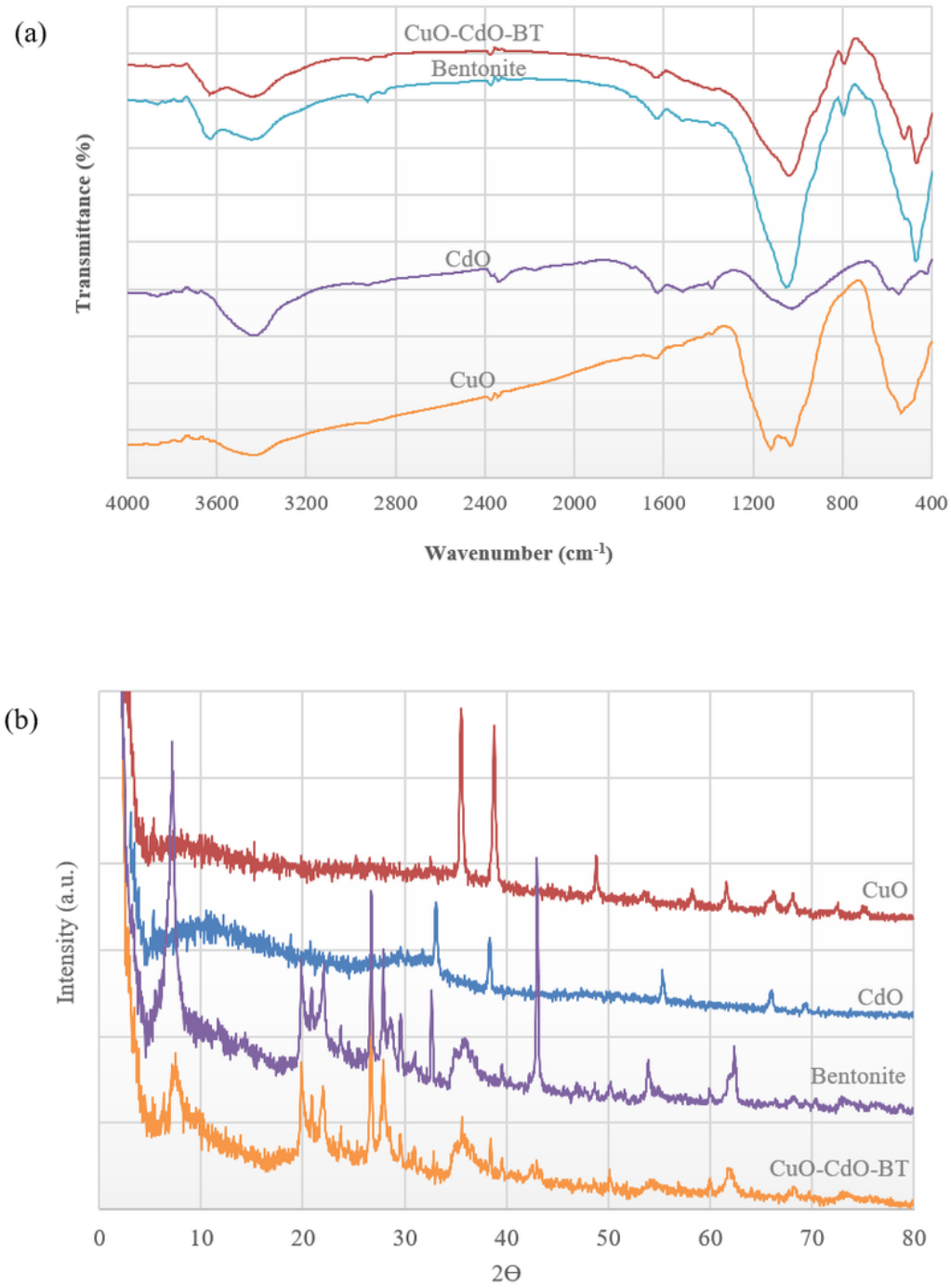


Figure 2

(a) FT-IR spectra and (b) XRD patterns of CuO-CdO-BT, bentonite, CuO NPs and CdO NPs

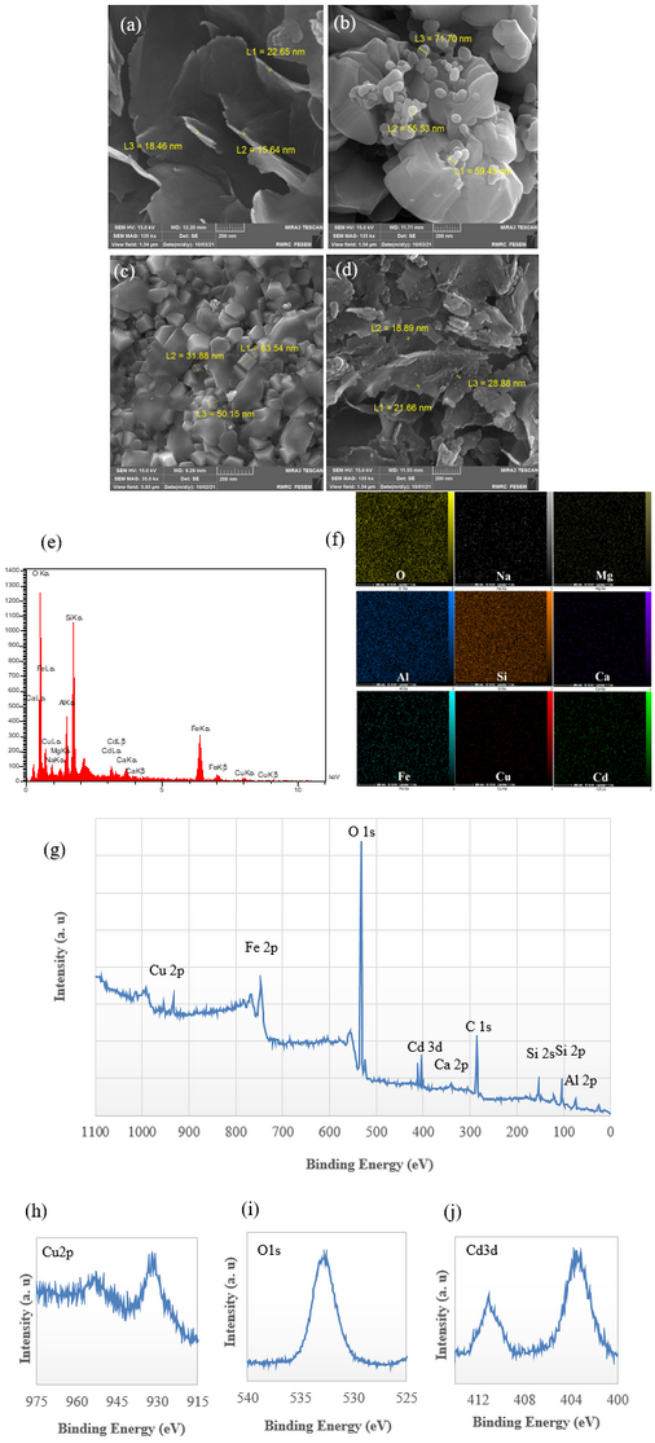


Figure 3

FE-SEM images of (a) raw bentonite, (b) CuO NPs, (c) CdO NPs, and (d) CuO-CdO-BT, (e) EDX spectrum of CuO-CdO-BT, (f) corresponding element mapping images of CuO-CdO-BT, XPS spectra of CuO-CdO-BT (g) survey, (h) Cu 2p, (i) O1s and (j) Cd3d

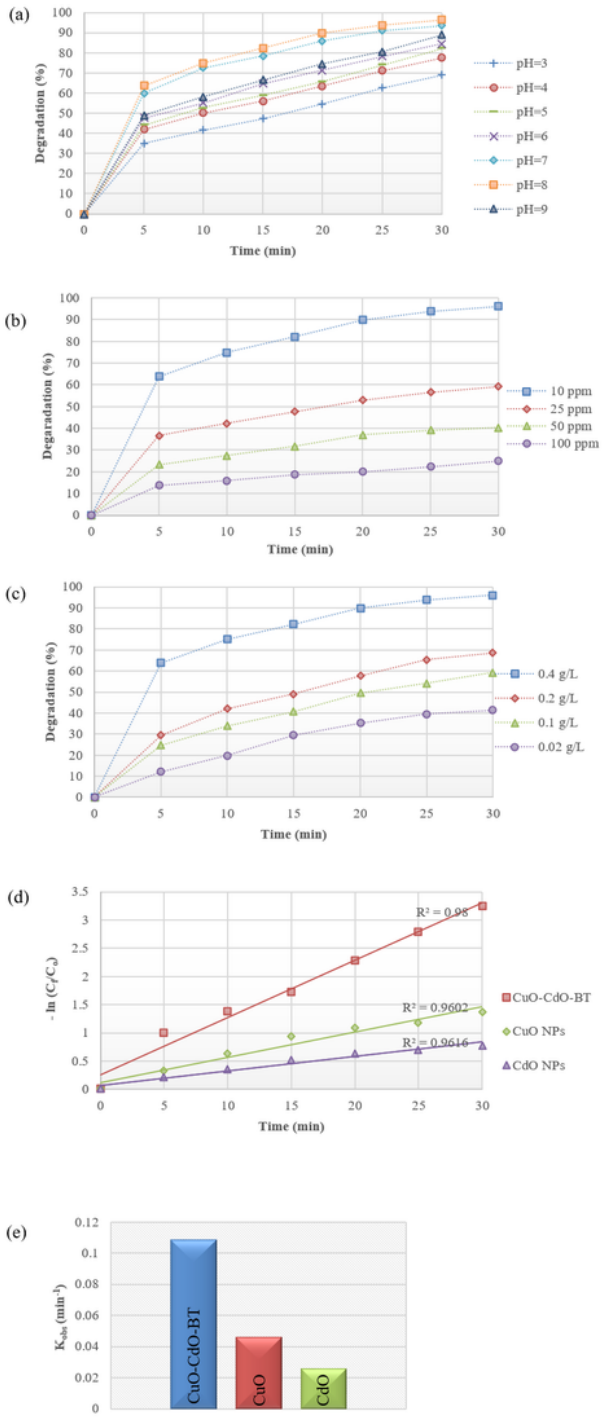


Figure 4

Photocatalytic degradation of LVF using CuO-CdO-BT at different (a) pH, (b) concentrations of antibiotic, (c) catalyst doses at pH=6 and (d) Pseudo-first-order kinetic model for degradation of LVF Photocatalytic degradation of LVF and (e) the corresponding k values in the presence of different catalysts.

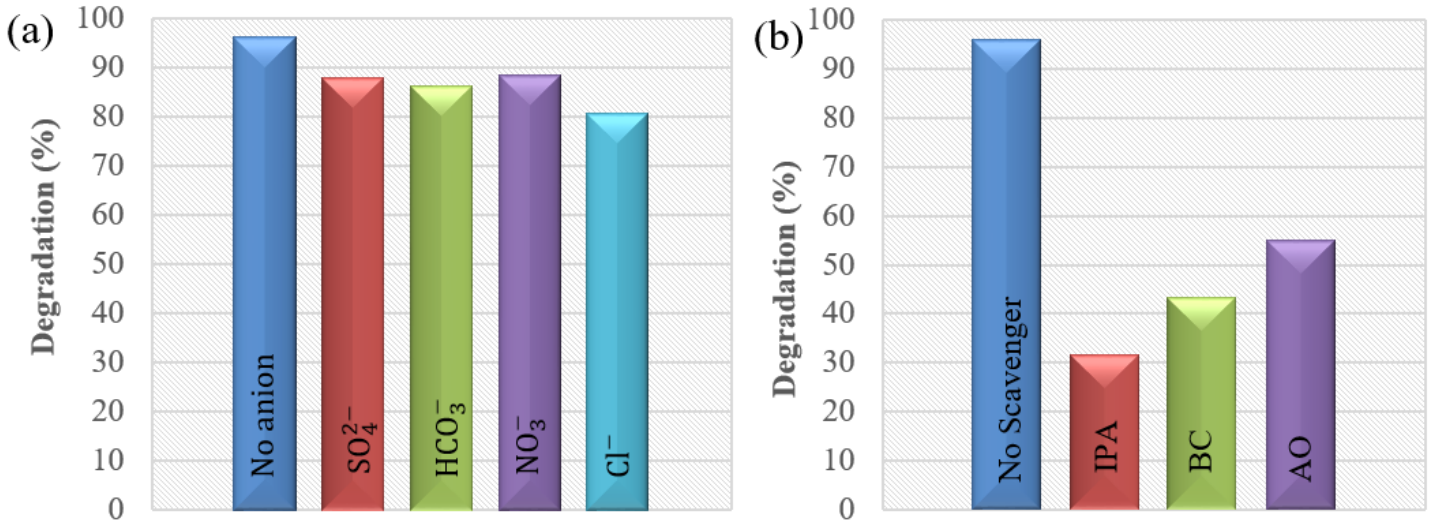


Figure 5

Photocatalytic degradation of LVF using CuO-CdO-BT in the presence of different (a) anions and (b) scavengers.

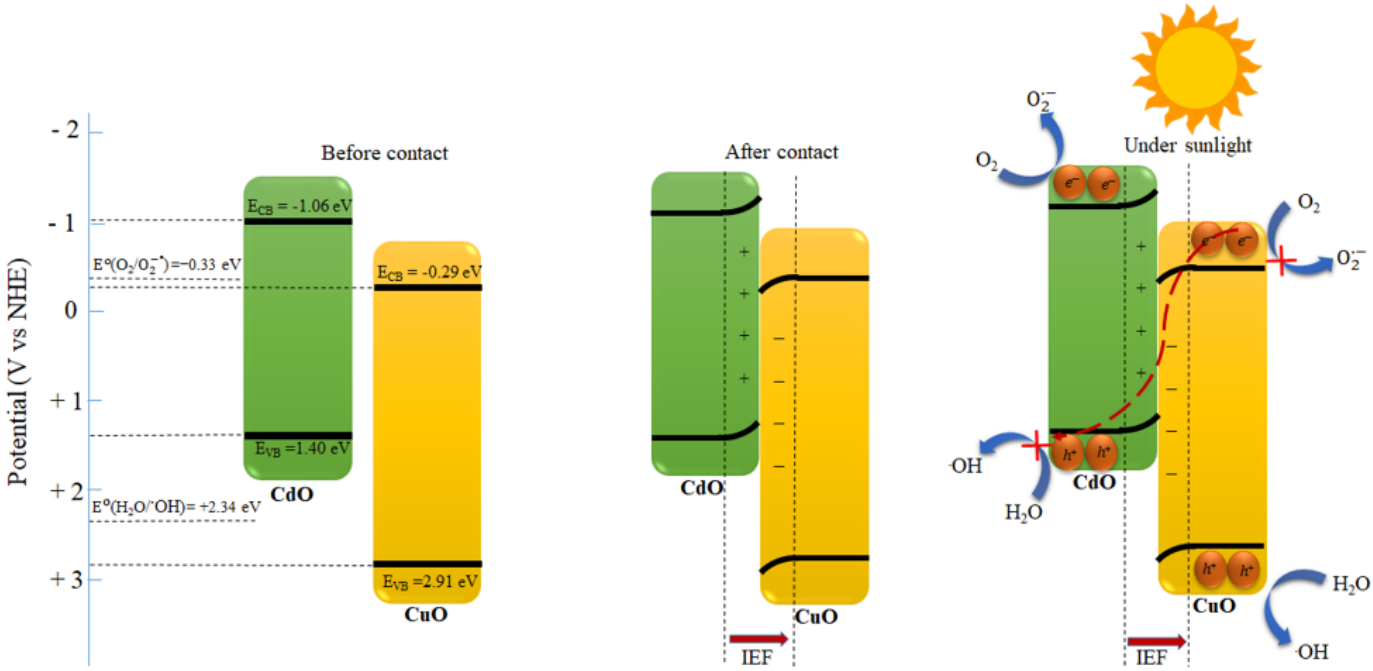


Figure 6

Schematic illustration of the S-scheme charge transfer process in the CuO-CdO-BT heterojunction

Supplementary Files

This is a list of supplementary files associated with this preprint. Click to download.

- Supplementrymaterial.docx
- Scheme1.png